# Tunneling anisotropic magnetoresistance in Co/AlO$_x$/Al tunnel junctions with fcc Co (111) electrodes

K. Wang,[1] T. L. A. Tran,[1] P. Brinks,[2] J. G. M. Sanderink,[1] T. Bolhuis,[1] W. G. van der Wiel,[1] and M. P. de Jong[1,*]
[1]*NanoElectronics Group, MESA + Institute for Nanotechnology, University of Twente, P.O. Box 217, Enschede 7500 AE, The Netherlands*
[2]*Faculty of Science and Technology, MESA + Institute for Nanotechnology, University of Twente, P.O. Box 217, Enschede 7500 AE, The Netherlands*
(Received 11 June 2013; published 9 August 2013)

Tunneling anisotropic magnetoresistance (TAMR) has been characterized in junctions comprised of face-centered cubic (fcc) Co (111) ferromagnetic electrodes grown epitaxially on sapphire substrates, amorphous AlO$_x$ tunnel barriers, and nonmagnetic Al counterelectrodes. Large TAMR ratios have been found, up to ∼7.5% and ∼11% (at 5 K), for the in-plane and out-of-plane magnetization geometry, respectively. Such large TAMR values were not expected *a priori*, given the weak anisotropy of the (bulk) Co bands due to spin-orbit interaction, and the absence of Co (111) surface states that cross the Fermi energy. Both the in-plane and out-of-plane TAMR effects exhibit a predominantly twofold symmetry, and a strong bias dependence. The in-plane TAMR shows a maximum along the (twofold) magnetic hard axis, suggesting a relation between magnetic anisotropy and TAMR. We propose that uniaxial strain in combination with Bychkov-Rashba spin-orbit interaction, producing an interfacial tunneling DOS that depends on the magnetization direction, is responsible for the TAMR effect. The importance of the interfacial Co/AlO$_x$ (electronic) structure for the TAMR effect is underlined by measurements on junctions with overoxidized AlO$_x$ barriers, which show markedly different bias and angle dependence.

DOI: 10.1103/PhysRevB.88.054407 PACS number(s): 85.75.−d, 75.76.+j, 75.70.Tj

## I. INTRODUCTION

In spintronics, the coupling between charge carrier spins and other degrees of freedom governing charge transport is exploited to obtain device functionalities ranging from magnetic field sensing to information storage and processing. In magnetic tunnel junctions (MTJs), a large resistance change (up to 600% at room temperature) can be obtained upon changing the relative alignment of the magnetization vectors of two ferromagnetic (FM) electrodes, separated by a tunnel barrier.[1] This effect, called tunnel magnetoresistance (TMR), arises because the density of states (DOS) in the ferromagnets is spin dependent, which results in different tunneling rates for majority versus minority spins. In turn, this produces a resistance that depends on the angle between the spin quantization axes (magnetization vectors) of the two ferromagnets.

Beyond these conventional TMR effects, the magnetoresistance (MR) of MTJs may also be varied via the rotation of the magnetization relative to different crystallographic axes of the ferromagnets,[2,3] or relative to the direction of current flow.[4] These effects are commonly referred to as tunneling anisotropic magnetoresistance (TAMR). Early studies have shown that the TAMR effect originates from spin-orbit interaction (SOI), which modulates the tunneling DOS as the magnetization direction changes.[5] TAMR effects may be expected whenever electron tunneling is affected by anisotropic spin-orbit fields, and have indeed been found for different systems including the aforementioned MTJs, single Co atoms adsorbed on Fe/W(110) surfaces,[6] and mechanically controlled break junctions.[7]

Unlike TMR, the TAMR effect persists in tunnel junctions that contain only one FM electrode. The first experimental evidence of the TAMR effect in spintronic devices was observed by Gould *et al*. for tunnel junctions comprised of a single ferromagnetic (Ga,Mn)As layer, an AlO$_x$ tunnel barrier, and a nonmagnetic Ti/Au counterelectrode.[2] Spin-valve-like device characteristics were observed, as well as a robust TAMR ratio of about 2.7% at 4.2 K. As (Ga,Mn)As has the zinc blende structure which lacks a center of inversion, it exhibits Dresselhaus SOI,[8] which, in combination with Bychkov-Rashba SOI (Ref. 9) originating from the interfaces, produces the TAMR.[10,11] This interplay between Dresselhaus- and Bychkov-Rashba SOI is present in all structures comprised of noncentrosymmetric materials, e.g., (Ga,Mn)As electrodes or GaAs barriers, and can explain the uniaxial symmetry of the in-plane TAMR that is typically observed for such structures.[3,10–15] Another class of junctions for which TAMR effects have been studied in some detail is MTJs that contain body-centered cubic (bcc) 3*d* ferromagnetic electrodes, e.g., Fe or CoFe. In these systems, resonant tunneling through surface states, influenced by Bychkov-Rashba SOI, has been put forward as an important mechanism to explain the experimental observations.[16–19] Localized surface states may mix with bulk bands, which produce so-called resonant surface bands.[20,21] Without Bychkov-Rashba SOI, e.g., for a highly symmetric MTJ configuration such as Co/vacuum/Co, theoretical analysis has shown that a large tunneling transmission through resonant states may be obtained due to the formation of bonding and antibonding hybrid states derived from the interface states on both sides of the barrier. In a tunnel junction comprised of a single ferromagnetic layer and a nonmagnetic metal as counterelectrode, the Bychkov-Rashba SOI can greatly enhance the admixture of surface and bulk bands which are eventually transferred into resonant bands.[16,18]

Since TAMR is due to SOI, large effects are expected and indeed found for systems in which heavy elements are present. Out-of-plane TAMR ratios in excess of 10% were observed at 4 K in junctions comprised of Pt-terminated stacks of Co/Pt ultrathin (1 nm) films.[22] This is much larger than the 0.15% TAMR value observed for similar stacks with Co termination,

 ©2013 American Physical Society

or the 0.4% effect found for Fe/GaAs/Au systems (both experiment and theory).[3] The difference has been attributed to the weak SOI in 3*d* ferromagnets compared to that in 5*d* transition metals.

In spite of the significant progress made regarding several specific systems described above, in particular those involving noncentrosymmetric materials such as GaAs, a detailed and generally applicable understanding of the mechanisms underlying TAMR is still lacking. Studies of systems that explore new areas of the "parameter space" determining the effects are therefore highly desirable. Here, we present an experimental TAMR study of junctions comprised of fcc Co (111) ferromagnetic electrodes grown epitaxially on sapphire substrates, amorphous $AlO_x$ tunnel barriers, and nonmagnetic Al counterelectrodes. We find large TAMR ratios up to ~7.5% and ~11% (at 5 K), for the in-plane and out-of-plane geometry, respectively. Such large TAMR values are surprising for several reasons. First, our junctions lack Dresselhaus SOI, and heavy elements with strong SOI are absent. Second, theoretical work concerning hexagonally close-packed (hcp) Co has predicted a weak SOI-induced anisotropy in the integrated bulk DOS at the Fermi energy, $E_F$, of 0.3% upon rotating the magnetization from [0001] to [1000].[23] Under the assumption of in-plane momentum conservation during tunneling, such that predominantly states with $\vec{k}$ along the tunneling direction are involved, the anisotropy in the tunneling DOS is calculated to be 1.3%. Based on these calculations, one would expect small TAMR ratios, on the order of 1% or less, in MTJs with a single ferromagnetic Co electrode. Third, contrary to the case of bcc Fe(001), hcp Co (0001) and also fcc Co (111) do not exhibit surface states that cross $E_F$.[24,25] Resonant tunneling through surface/interface states is therefore *a priori* not expected to play a significant role in tunnel junctions with hcp Co (0001) or fcc Co (111) electrodes.

The content of this paper is organized as follows. Section II provides the experimental details of this work. In Sec. III A, characterization of the structural and magnetic properties of the Co thin films is presented, by x-ray diffraction (XRD) and vibrating sample magnetometry (VSM) measurements, respectively. Section III B contains the results and discussion of magnetotransport measurements of $Co/AlO_x/Al$ junctions, focusing on in-plane and out-of-plane TAMR. Conclusions are presented in Sec. IV.

## II. EXPERIMENTAL DETAILS

All junctions were prepared by electron-beam evaporation in an ultrahigh vacuum (UHV, base pressure $10^{-10}$ mbar) system using shadow masks. One-side-polished monocystalline (0001) sapphire substrates, with an area of $11 \times 11$ mm$^2$, were cleaned in ultrasonic baths of acetone and isopropanol. Referring to Fig. 1(a), the epitaxial Co bottom layer of 8 nm thickness was grown on top of the sapphire substrate at room temperature, patterned into 5 mm × 2 mm strips using a stainless steel shadow mask. In order to achieve a thin $AlO_x$ tunnel barrier of uniform thickness, a 2.5-nm-thick Al layer was deposited on top of the Co thin film, after which the sample was transferred into the load-lock chamber for plasma oxidation (30 min in 100 mTorr $O_2$ at room temperature). This yields an $AlO_x$ tunnel barrier of 3.3 nm. Subsequently, $AlO_x$

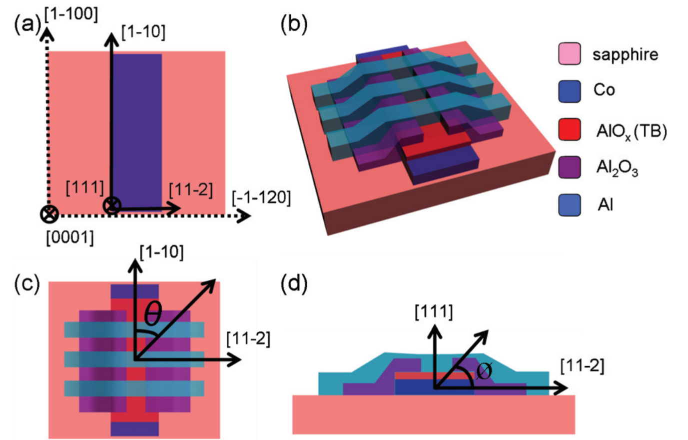


FIG. 1. (Color online) Schematic diagrams of (a) the epitaxial 8-nm Co thin film (patterned into 2 mm × 5 mm strips using shadow masking) on the single crystalline sapphire substrate at room temperature, with their in-plane crystallographic directions indicated; (b) the spintronic device with structure Co(8 nm)/$AlO_x$(3.3 nm)/Al(35 nm); (c) top view of such a tunnel junction, the angle $\theta$ indicates the in-plane magnetization direction with respect to the crystallographic axis [1-10]; (d) cross-sectional view of such a tunnel junction, the angle ø indicates the out-of-plane magnetization direction with respect to the crystallographic axis [11-2].

layers with a thickness of 30 nm were deposited through a shadow mask by *e*-beam evaporation of $Al_2O_3$, exposing a 250-$\mu$m-wide strip of the Co/tunnel-barrier stack. Finally, the Al top contacts were made by depositing 35-nm-thick Al strips of 300 $\mu$m width, resulting in cross bar structures with active junction areas of 250 $\mu$m × 300 $\mu$m. These structures are depicted in Fig. 1(b).

Magnetotransport measurements were carried out using a liquid helium flow cryostat equipped with a 1-T electromagnet. A four-terminal measurement geometry was used to minimize the contributions of the electrode resistances. The devices were mounted in a rotatable sample holder, enabling a 360° in-plane rotation of the magnetization of the Co thin films. Out-of-plane TAMR measurements were carried out using a physical properties measurement system (PPMS, Quantum Design), providing sufficiently large magnetic fields (up to 9 T) to saturate the out-of-plane magnetization of the 8-nm Co layer. The TAMR measurements were performed by injecting a constant direct current (dc) though the devices, while the voltage variations were recorded with a nanovolt meter. In addition to the magnetotransport measurements, the structural and magnetic properties of our Co thin films were characterized by XRD and VSM, respectively.

## III. RESULTS AND DISCUSSION

### A. Structural and magnetic properties of epitaxial Co films on sapphire (0001)

XRD measurements were carried out to determine the crystalline phases and the film-substrate epitaxial relations. Figure 2(a) shows the out-of-plane $\theta$-$2\theta$ scan of a 50-nm Co film on sapphire (0001). Four peaks can be observed, at $2\theta = 41.7°$, 44.4°, 90.8°, and 98.2°, respectively. Two peaks

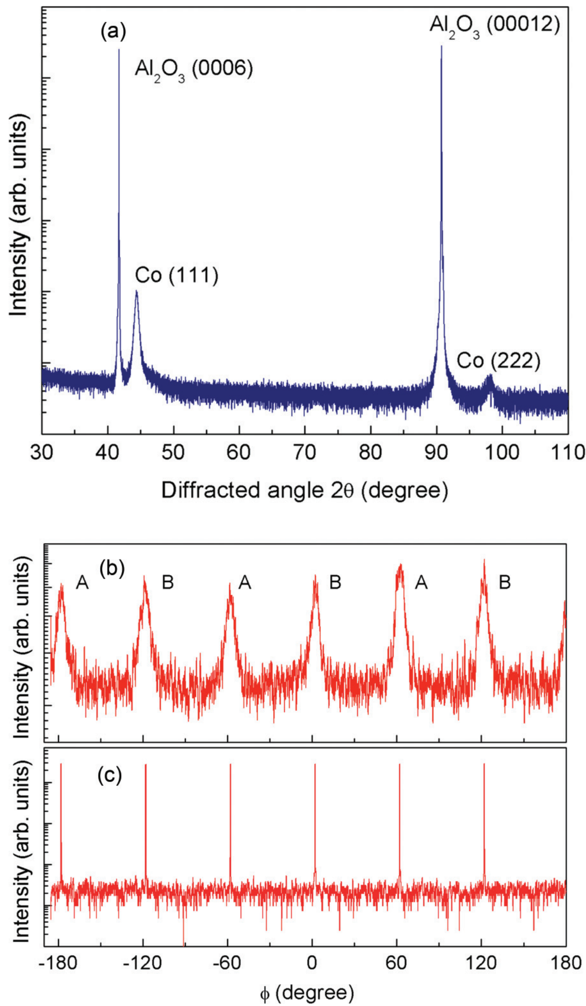


FIG. 2. (Color online) XRD spectra for a 50-nm Co thin film grown on sapphire (0001) substrate. (a) Out-of-plane $2\theta$-$\theta$ scan reveals fcc Co phases. (b) and (c) show the $\varphi$ scans of the fcc Co (11-1) planes, and the sapphire (11-23) planes, respectively.

with large intensities and narrow bandwidths appear at 41.7° and 90.8°, which are ascribed to the (0006) and (00012) diffraction peaks of the sapphire substrate, respectively. The peaks at 44.4° and 98.2° are attributed to the (111) and (222) signals of fcc Co. No other signals, due to impurity phases, could be detected. It can thus be concluded that the film, which was grown at room temperature, consists of solely fcc Co with a (111) orientation. This is consistent with previous reports concerning thin Co films on sapphire (0001), for which fcc Co (111) was found for growth temperatures below 150 °C, while coexisting fcc and hcp phases were obtained at higher temperatures.[26,27]

Further characterization of the fcc Co layer concerns the in-plane epitaxial relation with the substrate, using XRD $\varphi$ scans. The results are shown in Figs. 2(b) and 2(c), for both the fcc Co (11-1) planes, and the sapphire (11-23) planes, respectively. As can be seen from Figs. 2(b) and 2(c), six distinct diffracted peaks, with an equal adjacent angular spacing of 60°, are detected for both these planes, indicating a clear in-plane epitaxial relation. The epitaxial growth mode of the fcc Co thin film and the sapphire substrate is illustrated in

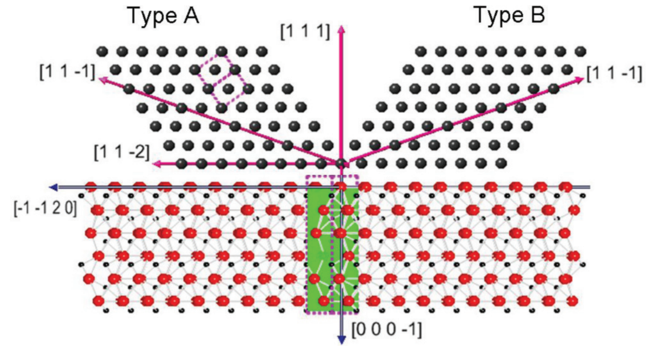


FIG. 3. (Color online) Schematic drawing of an fcc Co thin film grown on top of a (0001) sapphire substrate (green area indicates a unit cell of sapphire).

Fig. 3. Figure 3 shows a cross-sectional view of the modeled lattice structures of the fcc Co thin film grown on the sapphire substrate. In agreement with previous reports, the in-plane epitaxial relation can be understood from the following two types of crystallographic lattice arrangements:

$$\text{Type A}: \ \text{Co}\ (111)[1-10]_{\text{fcc}} \ || \ \text{Al}_2\text{O}_3\ (0001)[1-100],$$
$$\text{Type B}: \ \text{Co}\ (111)[-110]_{\text{fcc}} \ || \ \text{Al}_2\text{O}_3\ (0001)[-1100].$$

As shown in Fig. 3, the fcc Co film is comprised of two variants (i.e., types A and B), which are rotated around the film normal by 180° relative to each other. Such a lattice arrangement is similar to the cases of fcc Co films grown on MgO (111) and SrTiO3 (111).[26,28] We have defined and indexed the crystallographic orientations of the Co film and sapphire substrate, as shown in Figs. 1(a), 1(c), and 1(d). Summarizing, the XRD analysis indicates that the epitaxial Co thin film grown on sapphire (0001) consists of only fcc (111) phases, with a well-defined in-plane epitaxial orientation.

Figure 4 shows magnetic hysteresis loops, obtained by room-temperature VSM measurements, for an 8-nm Co thin film grown on a (0001) sapphire substrate. Two representative in-plane loops, which were measured along two perpendicular

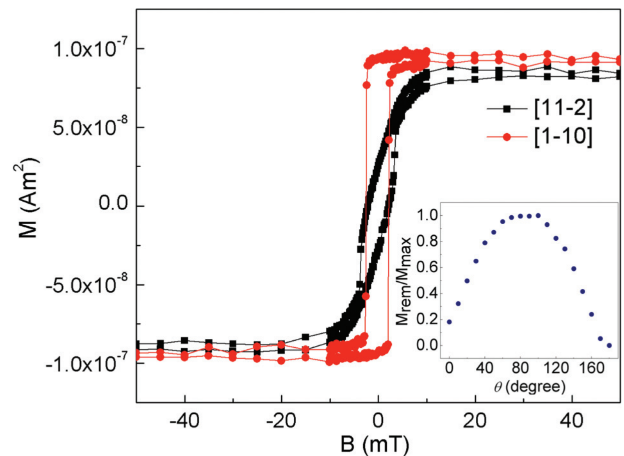


FIG. 4. (Color online) VSM measurements of an 8-nm Co thin film grown on a (0001) sapphire substrate at room temperature. The magnetic field was applied along the Co [1-10] and [11-2] in-plane directions. The inset shows the remnant magnetization as a function of the in-plane angle relative to the [11-2] crystallographic axis.

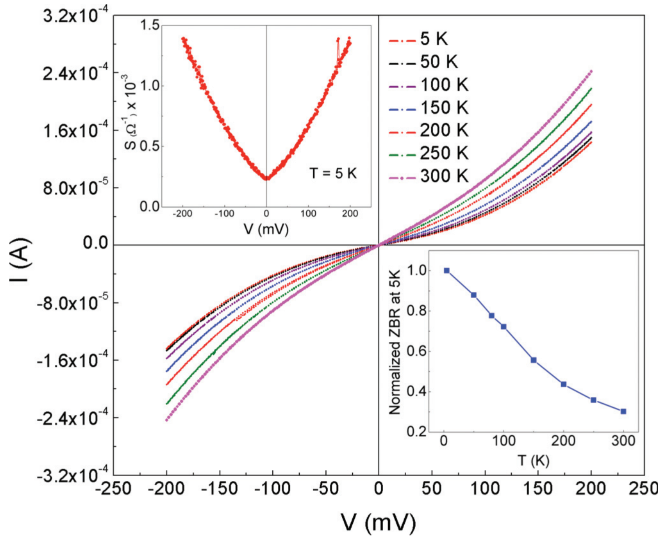


FIG. 5. (Color online) Temperature-dependent *I-V* measurements for Co(8 nm)/$AlO_x$(3.3 nm)/Al(35 nm) junctions. Left inset: the conductance versus voltage measured at 5 K. Right inset: temperature dependence of normalized zero bias resistance (NZBR).

crystallographic axes, are shown. The first was measured along the [1-10] direction and shows a square-shaped hysteresis loop with a coercivity of approximately 2.7 mT. By comparison, the second loop, which was measured along the [11-2] direction, exhibits a similar coercivity, but a more complex switching behavior and a significantly weaker magnetic remanence. The inset of Fig. 4 shows the normalized remanent magnetization measured with the magnetic field applied along different in-plane angles relative to the [1-10] direction, spanning a rotation of 180°. Clearly, the (as-prepared) Co thin film exhibits uniaxial magnetic anisotropy.

### B. Magnetotransport measurements

We first discuss the temperature dependence of the *I-V* characteristics to evaluate the basic electronic transport properties for our junctions, with the structure sapphire(0001)/Co (8 nm)/$Al_2O_3$ (3.3 nm)/Al (35 nm). Figure 5(a) shows the *I-V* curves of such a device, measured at seven different temperatures between 5 and 300 K. All *I-V* measurements exhibit supralinear and quasisymmetric behavior with respect to zero bias. From 5 to 300 K, the *I-V* curves show only a modest variation, consistent with tunneling as the dominating electronic transport mechanism. This is furthermore illustrated by the top inset of Fig. 5, depicting a conductance ($dI/dV$) curve that is typical for tunneling conduction. The temperature dependence of the normalized zero bias resistance (ZBR) displayed in the bottom inset of Fig. 5 shows weak insulatorlike behavior, which indicates a pinhole- and defect-free tunnel barrier.

TAMR measurements were performed at different temperatures, for both in-plane and out-of-plane configurations [see Figs. 1(c) and 1(d)]. As shown in Fig. 1(c), the in-plane TAMR measurements were carried out by rotating the magnetization direction with respect to a reference crystallographic axis of the Co thin film ($\theta = 0$ corresponds to the [1-10] direction). The magnetization was saturated along any in-plane direction by a applying a constant magnetic field of 500 mT. The in-plane TAMR ratio was evaluated as

$$\mathrm{TAMR}(\theta) = \frac{R(\theta) - R(0)}{R(0)}. \quad (1)$$

A similar procedure (and definition) for the TAMR (ø) was used for the out-of-plane configuration (a large constant magnetic field of 5 T was used to tilt the magnetization out of plane), as depicted in Fig. 1(d). ø = 0 is the direction along the [11-2] crystallographic axis. In spite of the apparent similarity, it should be pointed out that these two configurations correspond to rather different physical situations. In the case of the in-plane configuration, the current direction is always perpendicular to the magnetic field direction, and the anisotropy results from the anisotropic SOI in the Co lattice. By contrast, in the out-of-plane configuration, the orientation of the magnetization changes with respect to the direction of current flow (perpendicular to the tunnel barrier). In the latter case, but not in the former, a TAMR effect is observed even for structurally disordered ferromagnetic electrodes.

Figure 6(a) shows a contour plot of the in-plane TAMR, as a function of both injected current and angle $\theta$. The crystallographic axes corresponding to certain values of $\theta$ are indicated with labels/arrows. Clearly, the junction resistance is strongly influenced by not only the in-plane magnetization angle, but also the bias current. Note that the TAMR ratio is (nearly) always positive, meaning that the lowest junction resistance is obtained when the magnetization is along the [1-10] direction. The largest TAMR ratio observed is as high as ~7.5%. Figure 6(b) depicts the in-plane TAMR ratio as a function of bias current, measured at several different angles with respect to the reference crystallographic axis [1-10] of the Co thin film. The overall shapes of the curves are all fairly similar, showing a strongly decreasing TAMR effect as the bias increases, independent of the bias polarity. The applied bias current ranges from +5 to −5 $\mu$A across the junctions. This corresponds to a maximum bias voltage of approximately 16.6 and −16.4 mV, respectively, measured along the [1-10] crystallographic direction of the Co layer under an externally applied magnetic field of 500 mT. At higher bias, a larger region of the tunneling DOS is sampled, and the anisotropy with respect to the magnetization direction is integrated over a larger number of states. Therefore, the rapid suppression of the TAMR with increasing bias indicates that only electronic states close to $E_F$ exhibit a significant SOI-induced asymmetry, producing the TAMR. The same principle can also account for the strong temperature dependence of the TAMR effects in our junctions, which completely vanish above 100 K (not shown), since a broadening of the Fermi-Dirac distribution also leads to the sampling of a larger tunneling DOS. The TAMR curves in Fig. 6(b) also show a marked asymmetry for forward versus reverse bias. This asymmetry reflects the differences in the SOI for occupied versus unoccupied states at the Co/$AlO_x$ interface. It should be pointed out in passing that at constant bias current, the voltage across the junctions changes by a few percent when the magnetization direction is varied, such that a slightly different part of the tunneling DOS is probed. However, since significant changes of the TAMR effect occur only for much larger changes of the bias (see Fig. 6), this does not affect the interpretation of the data.

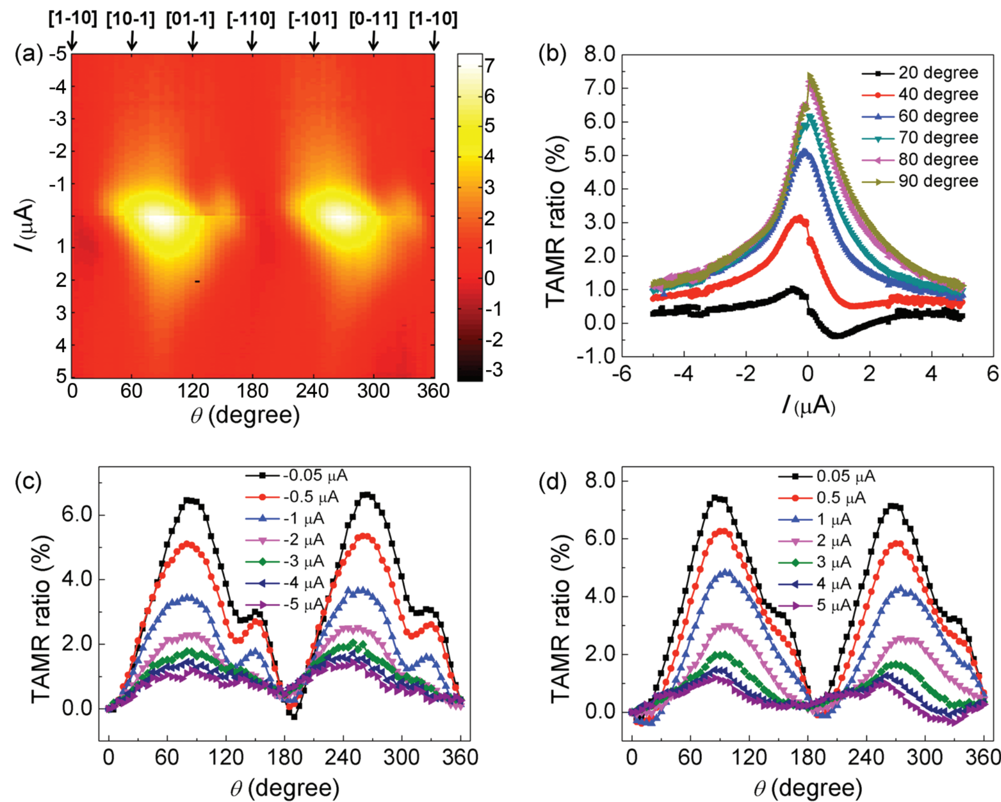


FIG. 6. (Color online) Devices were made with high-quality $AlO_x$ tunneling barriers. (a) Contour plot of the TAMR ratio as a function of both applied bias current and in-plane magnetization angle, measured at 5 K under application of a constant magnetic field of 500 mT. The color in the contour plot represents the magnitude of the TAMR ratio in percent (see color bar). (b) TAMR versus bias current for several different angles; (c) and (d) are angle-dependent TAMR for negative and positive bias current, respectively.

The decrease of the TAMR with bias is remarkably strong, when compared with other systems in which the bias dependence has been studied.[17,29] A notable exception is the very large (150 000%) TAMR effect observed in (Ga,Mn)As/GaAs/(Ga,Mn)As junctions,[14] which was found to rapidly decrease upon increasing the bias or temperature. In that case, the authors proposed that the large effect at low bias and low $T$ might be due to the formation of an Efros-Shklovskii gap upon crossing a metal-insulator transition,[30] which arises from Coulomb interactions between localized electrons in a disordered system. Such a scenario might be applicable indeed to (doped) semiconductor interfaces, but seems unlikely in our case. Disorder or defects in the barrier could also contribute to the rapid suppression of the TAMR upon increasing the bias or temperature, as also suggested in Ref. 14. However, as we conclude from the modest temperature dependence of the $IV$ curves, defect assisted tunneling does not play a significant role in our junctions. We note that a strong bias dependence has also been observed in $Co_{50}Fe_{50}/n$-GaAs junctions at 4.2 K, although in that study no data were presented for bias voltages below 10 mV.[31]

The plots of the TAMR as a function of $\theta$ shown in Figs. 6(c) and 6(d) reveal a predominantly twofold symmetry of the effect. Broad maxima are observed around $\theta \sim 90^\circ$ and $\sim 270^\circ$, corresponding to the [11-2] direction in the Co lattice, while two relatively weak shoulders appear at $\sim 140^\circ$ and $\sim 330^\circ$. These shoulders can only be observed at bias currents below $\pm 2\ \mu$A, corresponding to bias voltages of about $\pm 7$ mV. Based on the in-plane lattice symmetry for fcc Co(111), a sixfold symmetry of the TAMR is expected. Hence, we can exclude SOI-induced asymmetry of the bulk Co bands as the origin of the observed effects. We can also exclude interference between Bychkov-Rashba and Dresselhaus SOI, which was shown to result in a twofold symmetric in-plane TAMR effect in GaAs-based junctions, since our junctions do not contain noncentrosymmetric materials. In CoFe/MgO/CoFe and CoFe/$Al_2O_3$/CoFe junctions, the effect of Bychkov-Rashba SOI on interface states has been shown to produce TAMR with twofold as well as fourfold symmetry, depending on bias voltage.[17] Substituting the MgO barrier for an $Al_2O_3$ barrier produced strong changes in the TAMR effects for such junctions, underlining the importance of the interfaces. Therefore, for our junctions, the effects most probably also originate from the interfacial electronic structure.

To further investigate the influence of the interfacial properties on the TAMR, we analyzed junctions with a reduced thickness of the Al layer (2 nm) that forms the $AlO_x$ tunnel barrier after plasma oxidation. The plasma oxidation time was kept constant, however, such that the oxidation front penetrates somewhat into the Co film, producing a surplus of $CoO_x$ at the interface (the plasma oxidation procedure has been optimized previously, in terms of Al thickness versus oxidation time, using x-ray photoelectron spectroscopy). Such junctions exhibit a much smaller TAMR effect, with a markedly different dependence on bias as well as on the in-plane magnetization angle [see Figs. 7(a) and 7(b)]. In Figs. 7(c) and 7(d), at

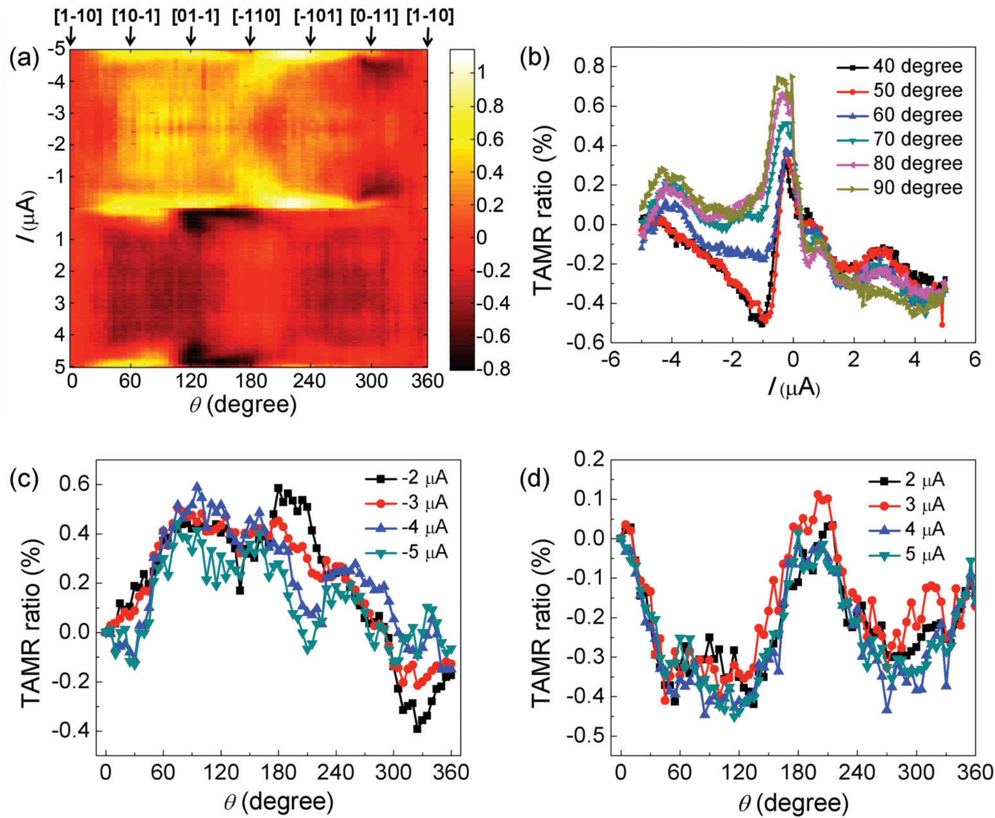


FIG. 7. (Color online) Devices were made with overoxidized $AlO_x$ tunneling barriers. (a) Contour plot of the TAMR ratio as a function of both applied bias current and in-plane magnetization angle, measured at 5 K under application of a constant magnetic field of 500 mT. The color in the contour plot represents the magnitude of the TAMR ratio in percent (see color bar). (b) TAMR versus bias current for several different angles; (c) and (d) are angle-dependent TAMR for negative and positive bias current, respectively.

positive bias, again a predominantly twofold TAMR effect is observed, while a much more complex angle dependence is found for negative bias. These measurements underline the importance of the interfacial (electronic) properties of the $Co/AlO_x$ contacts in determining the TAMR, its bias dependence, and its anisotropy.

It has been suggested that uniaxial strain in the epitaxial ferromagnetic layer may lead to TAMR with twofold symmetry.[11] This phenomenon has been previously proposed to be responsible for TAMR in epitaxial $(Ga,Mn)As/AlO_x/Au$ tunnel junctions.[2] Owing to the band hybridization and the SOI at the substrate/film interface, the substrate materials, as well as their crystalline orientations, have strong impact on the magnetic properties of thin films. Several previous studies have demonstrated uniaxial magnetic anisotropy in Co films fabricated on various substrates, such as single crystalline sapphire and Cu substrates. Notably, Co (0001) films grown on sapphire (11-20) have been shown to exhibit in-plane uniaxial anisotropy, which was attributed to the Co/sapphire interfacial structure.[32] In our case, VSM measurements also reveal uniaxial in-plane anisotropy (see Fig. 4). Our observation of twofold symmetric TAMR in combination with uniaxial in-plane anisotropy, where the TAMR maximum coincides with the in-plane hard axis, is suggestive of a common origin. A correlation between TAMR and magnetocrystalline anisotropy has also been found by others previously.[33] We therefore propose that uniaxial strain, combined with Bychkov-Rashba SOI, may play an important role in the TAMR in our junctions.

Figure 8 shows measurements of the out-of-plane TAMR effect, obtained at 5 K under application of a constant 5-T field. The maximum TAMR observed is ~11%, which is similar to that observed for CoPt-based junctions.[22] Similar to the in-plane TAMR effect, a strong reduction of the TAMR ratio with increasing bias current is observed [Fig. 8(a)]. Figures 8(b) and 8(c) show that the TAMR increases as the magnetization changes from the in-plane (i.e., [11-2]) to the out-of-plane (i.e., [111]) direction, for both negative and positive bias currents.

It has been proposed that the Bychkov-Rashba SOI is also responsible for the out-of-plane TAMR of MTJs with asymmetric structures. The potential gradient along the growth direction (with the addition of externally applied electric fields) generates an effective Bychkov-Rashba SOI field,

$$W_{\mathrm{BR}} = (-\alpha k_y, -\alpha k_x, 0), \tag{2}$$

where $\alpha$ is the Bychkov-Rasha SOI parameter; and $k_x$ and $k_y$ are the in-pane wave vectors. The rotation of the magnetization from in plane to out of plane causes an energy shift equal to

$$\Delta E_{\uparrow\downarrow} = \pm W_{\mathrm{BR}} M. \tag{3}$$

Thus, the energy bands become anisotropic in response to the magnetization direction. In the present case, $\Delta E_{\uparrow\downarrow}$ vanishes when $\boldsymbol{M}$ is perpendicular to the Co layer (i.e., at $\phi = 90^\circ$, such that $\boldsymbol{M}$ is along the [111] crystallographic direction of

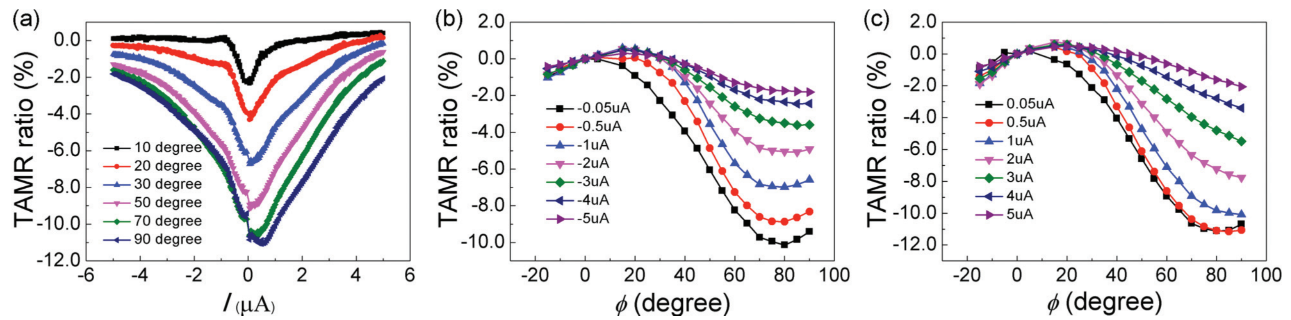


FIG. 8. (Color online) Out-of-plane TAMR signals, measured at 5 K under application of a constant magnetic field of 5 T. (a) Bias current dependence of the out-of-plane TAMR effect. (b) and (c) show the angle dependence of the out-of-plane TAMR effects measured at negative and positive bias currents, respectively.

Co), while it retains a finite value for ø between 0° and 90°. This implies that the TAMR effect follows the relations TAMR(ø) = TAMR(ø + 180°), and is consistent with the twofold symmetry observed in the experiments.

## IV. CONCLUSIONS

We have observed large TAMR effects in Co/$AlO_x$/Al tunnel junctions comprised of fcc Co (111) electrodes, which is unexpected based on the small SOI-induced anisotropy of the bulk DOS predicted by theory. XRD measurements demonstrated growth of epitaxial (111) fcc Co thin films on single crystalline (0001) sapphire substrates at room temperature. This growth mode for Co leads to uniaxial in-plane magnetic anisotropy, as shown by VSM measurements. Co(8 nm)/$AlO_x$(3.3 nm)/Al(35 nm) junctions showed clean tunneling behavior, with a weak temperature dependence, indicating that defect assisted tunneling does not play a significant role. TAMR ratios in excess of 7.5% and 11% are found at 5 K for the in-plane and out-of-plane geometry, respectively. Both the in-plane and out-of-plane effects exhibit twofold symmetry. The in-plane TAMR shows a maximum along the in-plane magnetic hard axis, suggesting a relation between magnetic anisotropy and TAMR. We propose that uniaxial strain in combination with Bychkov-Rasba SOI, producing an interfacial tunneling DOS that depends on the magnetization direction, is responsible for the TAMR. The crucial role played by the Co/$AlO_x$ interface is underlined by TAMR measurements of junctions with overoxidized $AlO_x$ barriers (and therefore a surplus of $CoO_x$ at the interface), showing markedly different bias and angle dependence.


## ACKNOWLEDGMENTS

We acknowledge financial support from the European Research Council (ERC Starting Grants No. 280020 and No. 240433), and the research program of the Foundation for Fundamental Research on Matter (FOM, Grant No. 10PR2808), which is part of the Netherlands Organization for Scientific Research (NWO).


*Corresponding author: m.p.dejong@utwente.nl


[1] S. Ikeda, J. Hayakawa, Y. Ashizawa, Y. M. Lee, K. Miura, H. Hasegawa, M. Tsunoda, F. Matsukura, and H. Ohno, Appl. Phys. Lett. **93**, 082508 (2008).

[2] C. Gould, C. Ruster, T. Jungwirth, E. Girgis, G. M. Schott, R. Giraud, K. Brunner, G. Schmidt, and L. W. Molenkamp, Phys. Rev. Lett. **93**, 117203 (2004).

[3] J. Moser, A. Matos-Abiague, D. Schuh, W. Wegscheider, J. Fabian, and D. Weiss, Phys. Rev. Lett. **99**, 056601 (2007).

[4] L. Brey, C. Tejedor, and J. Fernandez-Rossier, Appl. Phys. Lett. **85**, 1996 (2004).

[5] M. Bode, S. Heinze, A. Kubetzka, O. Pietzsch, X. Nie, G. Bihlmayer, S. Blügel, and R. Wiesendanger, Phys. Rev. Lett. **89**, 237205 (2002).

[6] N. Néel, S. Schröder, N. Ruppelt, P. Ferriani, J. Kröger, R. Berndt, and S. Heinze, Phys. Rev. Lett. **110**, 037202 (2013).

[7] M. Viret, M. Gabureac, F. Ott, C. Fermon, C. Barreteau, G. Autes, and R. Guirado-Lopez, Eur. Phys. J. B **51**, 1 (2006).

[8] G. Dresselhaus, Phys. Rev. **100**, 580 (1955).

[9] Y. A. Bychkov and E. I. Rashba, J. Phys. C **17**, 6039 (1984).

[10] A. Matos-Abiague and J. Fabian, Phys. Rev. B **79**, 155303 (2009).

[11] A. Matos-Abiague, M. Gmitra, and J. Fabian, Phys. Rev. B **80**, 045312 (2009).

[12] M. Ciorga, M. Schlapps, A. Einwanger, S. Geissler, J. Sadowski, W. Wegscheider, and D. Weiss, New J. Phys. **9**, 351 (2007).

[13] M. Wimmer, M. Lobenhofer, J. Moser, A. Matos-Abiague, D. Schuh, W. Wegscheider, J. Fabian, K. Richter, and D. Weiss, Phys. Rev. B **80**, 121301 (2009).

[14] C. Rüster, C. Gould, T. Jungwirth, J. Sinova, G. M. Schott, R. Giraud, K. Brunner, G. Schmidt, and L. W. Molenkamp, Phys. Rev. Lett. **94**, 027203 (2005).

[15] C. Gould, K. Pappert, G. Schmidt, and L. W. Molenkamp, Adv. Mater. **19**, 323 (2007).

[16] A. N. Chantis, K. D. Belashchenko, E. Y. Tsymbal, and M. van Schilfgaarde, Phys. Rev. Lett. **98**, 046601 (2007).

[17] L. Gao, X. Jiang, S.-H. Yang, J. D. Burton, E. Y. Tsymbal, and S. S. P. Parkin, Phys. Rev. Lett. **99**, 226602 (2007).

[18] M. N. Khan, J. Henk, and P. Bruno, J. Phys.: Condens. Matter **20**, 155208 (2008).

[19] Y. Lu, H.-X. Yang, C. Tiusan, M. Hehn, M. Chshiev, A. Duluard, B. Kierren, G. Lengaigne, D. Lacour, C. Bellouard, and F. Montaigne, Phys. Rev. B **86**, 184420 (2012).

[20]O. Wunnicke, N. Papanikolaou, R. Zeller, P. H. Dederichs, V. Drchal, and J. Kudrnovský, Phys. Rev. B **65**, 064425 (2002).
[21]K. D. Belashchenko, J. Velev, and E. Y. Tsymbal, Phys. Rev. B **72**, 140404 (2005).
[22]B. G. Park, J. Wunderlich, D. A. Williams, S. J. Joo, K. Y. Jung, K. H. Shin, K. Olejník, A. B. Shick, and T. Jungwirth, Phys. Rev. Lett. **100**, 087204 (2008).
[23]A. B. Shick, F. Máca, J. Mašek, and T. Jungwirth, Phys. Rev. B **73**, 024418 (2006).
[24]M. A. Barral, M. Weissman, and A. M. Llois, Phys. Rev. B **72**, 125433 (2005).
[25]F. Gimbert, L. Calmels, and S. Andrieu, Phys. Rev. B **84**, 094432 (2011).
[26]M. Ohtake, O. Yabuhara, Y. Nukaga, and M. Futamoto, in *Joint European Magnetic Symposia*, edited by J. Spalek, Vol. 303 (Iop Publishing Ltd, Bristol, 2011), p. 012016.
[27]O. Yabuhara, M. Ohtake, Y. Nukaga, and M. Futamoto, in *2nd International Symposium on Advanced Magnetic Materials and Applications*, edited by M. Takahashi, H. Saito, S. Yoshimura, K. Takanashi, M. Sahashi, and M. Tsunoda, Vol. 266 (Iop Publishing Ltd, Bristol, 2011), p. 012049.
[28]O. Yabuhara, Y. Nukaga, M. Ohtake, F. Kirino, and M. Futamoto, J. Magn. Soc. Jpn. **34**, 78 (2010).
[29]R. Giraud, M. Gryglas, L. Thevenard, A. Lemaitre, and G. Faini, Appl. Phys. Lett. **87**, 242505 (2005).
[30]A. L. Efros and B. I. Shklovskii, J. Phys. C **8**, L49 (1975).
[31]T. Uemura, M. Harada, T. Akiho, K.-i. Matsuda, and M. Yamamoto, Appl. Phys. Lett. **98**, 102503 (2011).
[32]N. Metoki, T. Zeidler, A. Stierle, K. Bröhl, and H. Zabel, J. Magn. Magn. Mater. **118**, 57 (1993).
[33]H. Saito, S. Yuasa, and K. Ando, Phys. Rev. Lett. **95**, 086604 (2005).